Metal-enhanced fluorescence from tin nanostructured surfaces

Yongxia Zhang, Anatoliy Dragan, and Chris D. Geddes[a)]
Institute of Fluorescence, Laboratory for Advanced Medical Plasmonics, and Laboratory for Advanced Fluorescence Spectroscopy, University of Maryland Biotechnology Institute, 701 East Pratt St, Baltimore, Maryland 21202, USA

(Received 6 July 2009; accepted 3 December 2009; published online 20 January 2010)

The recent surge in interest in the metal-enhanced fluorescence (MEF) phenomenon and its numerous applications in the biosciences has fueled research into identifying alternative metals to silver which have desirable properties, such as enhanced emission and fluorophore photostability. In this paper, we subsequently study and reveal that tin nanodeposits are a suitable metal for MEF with an electric field wavelength dependence somewhat different than silver. An enhanced fluorescence emission coupled with a reduced fluorophore lifetime suggests both an electric field and plasmon-coupling component are the underlying mechanisms for tin-based MEF. In addition, an enhanced fluorophore photostability is observed near-to tin nanodeposits.
 [doi:10.1063/1.3284081]

I. INTRODUCTION

Fluorescence detection is the dominant tool in medical diagnostics and biotechnology today.[1–5] While fluorescence can be a very sensitive technique, the detection limit is usually limited by the quantum yield of the fluorophore (label), the autofluorescence of the sample, and the photostability of the fluorophores. In this regard, metallic nanostructures have been used to favorably modify the spectral properties of fluorophores and to alleviate some of their more classical photophysical constraints. The use of fluorophore-metal interactions has been termed metal-enhanced fluorescence (MEF) by Geddes and Lakowicz.[6] To date, MEF from plasmonic nanostructured materials such as silver,[7] gold,[8] copper,[9] zinc,[10] chromium,[11] and nickel[12] have been observed by our laboratory. In this regard, silver, gold, and copper nanoparticles were used for applications of MEF with fluorophores emitting in the visible wavelength region, while zinc and chromium nanostructured films were shown to additionally enhance the fluorescence emission of fluorophores in the UV and blue spectral regions, where as nickel was shown to enhance in the near infrared spectral range.[12] In this paper we subsequently show that tin nanodeposited films can also be used as substrates for MEF applications. Tin nanodeposits of various thicknesses were deposited using thermal vapor deposition onto glass microscope slides, which were characterized by optical absorption and atomic force microscopy (AFM) techniques. Enhanced fluorescence emission from fluorophores was observed for fluorophores near-to the tin deposits. In addition, we have observed a shorter fluorescence lifetime for fluorophores, which is in complete agreement with other reports and trends for MEF from other metals such as silver, which also shows a reduced coupled system lifetime, suggesting that both an enhanced electric field and a plasmon-coupling component underpins the mechanism for fluorescence enhancement.

a)Author to whom correspondence should be addressed. Electronic mail: geddes@umbi.umd.edu.

II. EXPERIMENTAL SECTION

Materials. Fluorescein was obtained from Sigma-Aldrich Chemical company and used as received. Silane prep™ glass microscope slides were purchased from Sigma-Aldrich. Tin nanostructured films of various thicknesses were deposited onto silane-prep™ glass microscope slides using thermal vapor deposition, AccuCoat, Inc. Rochester, NY, USA.

Preparation of sandwich format samples for MEF measurements. A solution of 100 μl of a fluorophore (10 μM) was sandwiched between two glass slides for the control sample and between one glass and one tin nanostructured film. Fluorescein was excited with a cw laser source at 455 nm and the fluorescence emission spectra measured as described as below.

Fluorescence lifetime analysis. Fluorescence lifetimes were measured using the time-correlated single photon counting technique, a Horiba Jobin Yvon fluorescence lifetime spectrometer (TemPro) with a 444 nm NanoLED as the light source. The intensity decays were analyzed in terms of the multiexponential model

$$I(t) = \sum_i \alpha_i \exp(-t/\tau_i), \tag{1}$$

where α_i are the amplitudes and τi are the decay times, $\Sigma_i \alpha i = 1.0$. The fractional contribution of each component to the steady-state intensity is given by

$$f_i = \frac{\alpha_i \tau_i}{\sum_j \alpha_j \tau_j}. \tag{2}$$

The mean lifetime of the excited state is given by

$$\bar{\tau} = \sum_i f_i \tau_i \tag{3}$$

and the amplitude-weighted lifetime is given by

$$\langle \tau \rangle = \sum_i \alpha_i \tau_i. \tag{4}$$

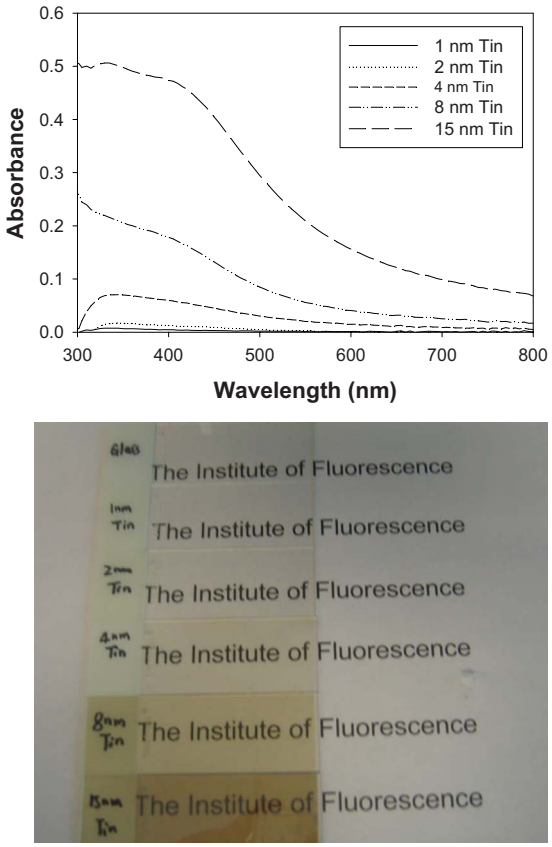

FIG. 1. (Color online) Absorption spectrum of vapor deposited metallic tin of various thicknesses deposited onto glass slides (top). The photograph of glass and tin slides with different thicknesses 1, 2, 4, 8, and 10 nm (bottom), demonstrating the semitransparent nature of the films.

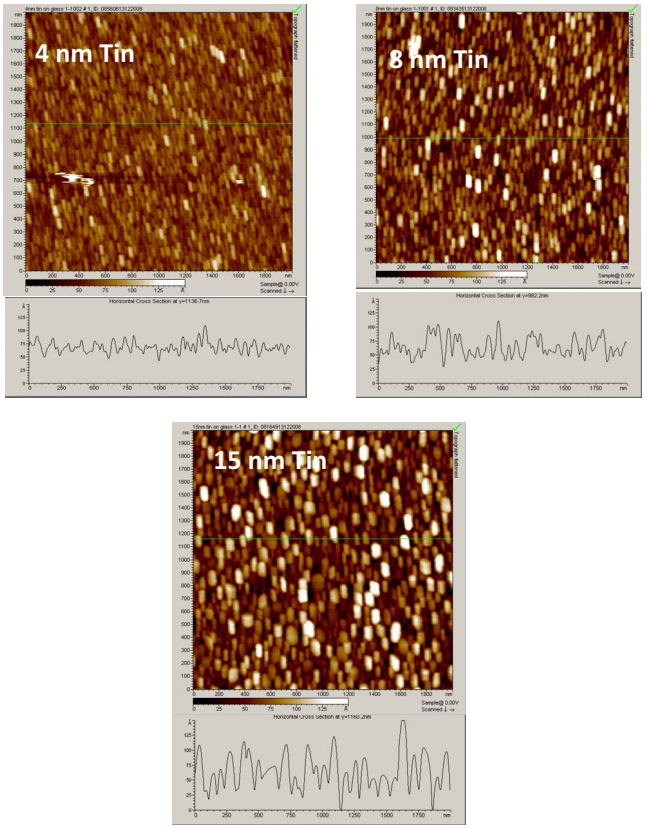

FIG. 2. (Color online) AFM images of 4, 8, and 15 nm Sn on glass. Below are the respective line scans for the AFM images.

The values of α_i and τ_i were determined by a nonlinear least-squares impulse reconvolution with a goodness-of-fit X^2 criterion.

Optical spectroscopy. The absorption spectra of the tin nanostructured films of varying thicknesses were collected using a Varian Cary 50 UV-Vis spectrophotometer. Fluorescence spectra of the fluorophores were measured with blank glass sandwiches and glass-nanostructured film sandwiches using an Ocean Optics HD2000 fluorometer.

AFM. AFM images were performed on a molecular imaging picoplus microscope. Samples were imaged at a scan rate of 1 Hz with 512×512 pixel resolution in a tapping mode.

Finite-difference time-domain (FDTD) calculations. The FDTD method was employed here to determine the electric field intensities and distributions at the surface of tin nanoparticles in a total field scattered field (TFSF). TFSF sources are used to divide the computation area or volume into total field (incident plus scattered field) and scattered field only regions. The incident *p*-polarized electric field is defined as a plane wave with a wave vector that is normal to the injection surface. The scattered and total fields were monitored during the simulation such that the total or scattered transmission can be measured. Using LUMERICAL (Canada) FDTD solution software, the simulation region was set to $800 \times 800 \times 800$ nm with a mesh accuracy of six. The overall simulation time was set to 500 ns and calculated over a frequency range from 300 to 800 nm for silver nanoparticles and 300–800 nm for the tin nanoparticles.

III. RESULTS AND DISCUSSION

Figure 1 shows the absorption spectra of 1, 2, 4, 8, and 15 nm thickness tin nanodeposits. Tin nanodeposits of 1, 2, and 4 nm show an absorbance peak around 340 nm. With increasing thickness, a broad absorption spectrum was observed, which is indicative of the aggregation and close proximity of the nanodeposits on the surface. In Fig. 1 (bottom), the different thickness tin deposits show their transparency with decreased loading. The morphology of different thickness of nickel films was measured by AFM. AFM images of 4, 8, and 15 nm Sn film are shown in Fig. 2. For the 15 nm tin film, the height of islands was ≈7 mm, as seen from the line scan results. For the 8 nm Sn film, the height of the Sn particles was ≈5 mm. For the 4 nm Sn film, the height of the Sn particles was around 2 nm. From the thickness of the Sn film also measured using the quartz crystal microbalance in the thermal vapor deposition unit, it can be concluded that there are multilayers of the Sn nanoparticles on the glass slides and Sn nanoparticles grow larger with increasing thickness, or extent of surface loading.

To test the tin deposits for potential applications in MEF, the fluorescence emission spectra of fluorescein in water on different thickness Sn films and on glass were measured as shown in Fig. 3. It can be seen that the fluorescence of fluorescein is enhanced (≈2.5 fold) for 15 nm Sn, where the enhancement factor increased with increased Sn thickness

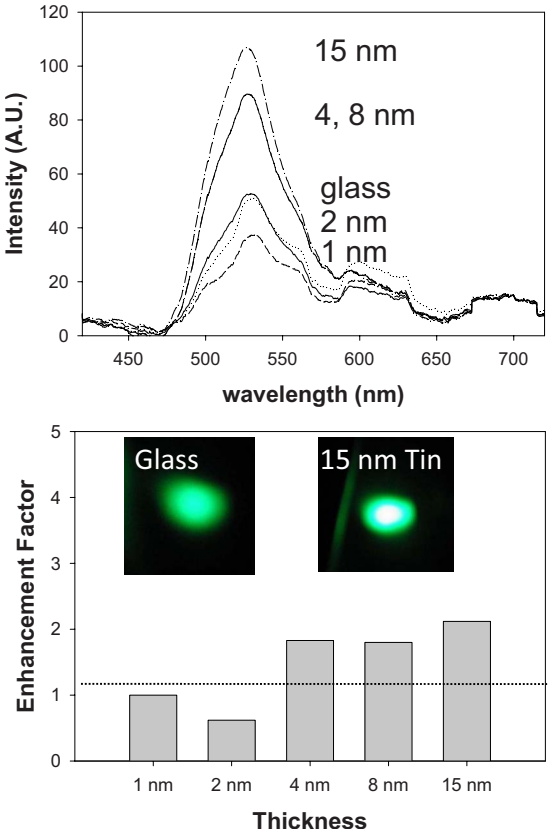

FIG. 3. (Color online) Emission spectra (top) and fluorescence enhancement factor (bottom) for a solution of fluorescein in water sandwiched between glass and tin slides of varying thicknesses. Ex: 455 nm, filter 500 nm long-pass. The enhancement factors were determined from several measurements on the film surface.

TABLE I. Fluorescence lifetime of fluorescein in water (pH=7.0) and on tin nanodeposits measured using time domain fluorometry. $\langle\tau\rangle$: the amplitude-weighted lifetime. $\bar{\tau}$: the mean lifetime. The experimental geometry of samples (top left) and schematic representation of metal-enhanced fluorescence (top right).

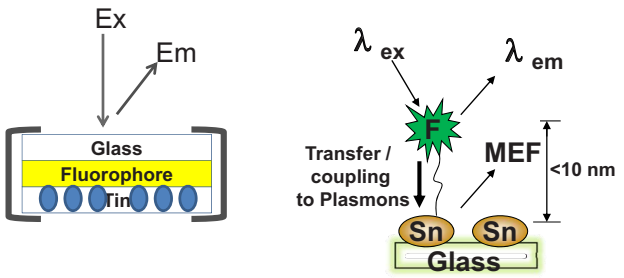

	τ (ns)	A%	τ (ns)	A2%	< τ> ns	$\bar{\tau}$ ns	χ^2
Fluorescein in H_2O in cuvette	3.9	100			3.9	3.9	1.0
Fluorescein glass/glass sandwich	3.5	78.9	7.6	21.1	3.9	4.1	1.2
Fluorescein 4 nm Tin/ glass	3.8	76	4.1	24	3.8	3.8	0.9
Fluorescein 8 nm Tin/ glass	3.4	60	3.6	40	3.5	3.5	0.9
Fluorescein 15 nm Tin/ glass	3.1	40	3.6	60	3.4	3.4	1.2

(Fig. 3, bottom). The fluorescence was diminished when the tin (Sn) thickness was smaller than 4 nm. It is well known that the absorption (C_A) and scattering (C_s) portions of a metallic nanoparticles extinction C_E underpin both the enhanced absorption and enhanced emission effects which cumulatively account for the enhancement factors in MEF.[13]

$$C_E = C_A + C_S = k_1\ \mathrm{Im}(\alpha) + \frac{k_1^4}{6\pi}|\alpha|^2, \tag{5}$$

where $k_1 = 2\pi n_1/\lambda_o$ is the wave vector of the incident light in the surrounding medium (typically, air, water, or polymer film), α is the polarizability of the sphere with radius r, n_1 is the refractive index of the medium, and λ_o is the incident wavelength. The term $|\alpha|^2$ is the square of the modulus of α

$$\alpha = 4\pi r^3(\varepsilon_m - \varepsilon_1)/(\varepsilon_m + 2\varepsilon_1), \tag{6}$$

where ε_1 and ε_m are the dielectric and the complex dielectric constants of the media and the metal, respectively. Given that the absorption component scales as the radius cubed and the scattering component scales as the radius to the sixth power, it is therefore expected that close-proximity fluorophores would demonstrate more enhanced properties near-to larger nanoparticles. This finding is consistent with trends observed for continuous and particulate silver and gold films and their influence on MEF.[8,14] The real-color photograph inserts (Fig. 3, bottom insert) also provide additional visual evidence for enhanced emission from the Sn film. In this regard, it should be noted that the true MEF enhancement factor (I Sn/I glass) is actually ≈125 fold. This is because the MEF phenomenon is through space interaction with fluorophore-particle coupling at distances less than 20 nm. Given that the MEF enhancement originates from only the first 20 nm of solution in a 1 μm solution sandwich, then the observed ≈2.5-fold enhancement originates from only 2% of the total sample volume, with an effective enhancement therefore of nearly 125 fold. Table I (top) shows the metal enhanced sandwich experimental geometry used in this study.

The photostability of fluorescein on a 15 nm tin film was also measured. Figure 4 shows fluorescein emission as a function of time, excited at 455 nm and observed through a 500-nm-long pass filter. The relative intensities of the plots reflect that more detectable photons can be observed per unit time from the 15 nm tin film, as compared to glass (a control sample), where the integrated areas under the plots is proportional to the photon flux from the respective samples. By additionally adjusting the laser power to match the same initial steady-state intensities of the samples, the fluorescein on tin can be seen to be more photostable. This finding suggests that the lifetime of the fluorescein is shorter on 15 nm tin film, the fluorescein in essence spending less time on average in an excited state due to the fast nonradiative energy transfer to the tin, and therefore is less prone to photo destruction, i.e., is more photostable.

In this regard, we have also measured the time-resolved intensity decays of fluorescein (fluorescence lifetimes) in

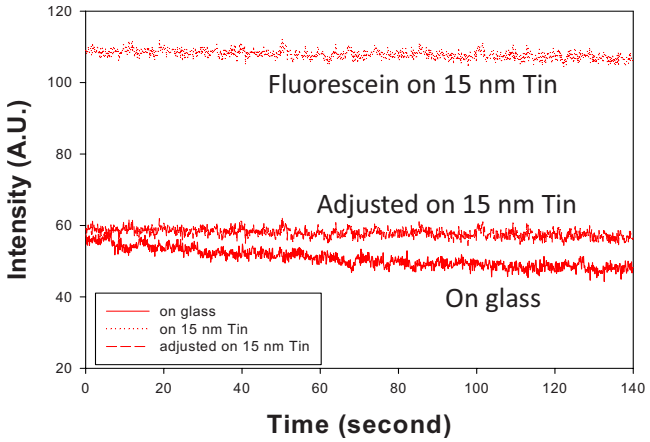

FIG. 4. (Color online) Emission intensity vs time of fluorescein on 15 nm tin and glass with constant 455 nm excitation (top curve), and with the laser power adjusted to give the same initial steady-state fluorescence intensity as that observed on glass (middle). Bottom trace shows the emission intensity of fluorescence vs time for a sandwich solution on glass slides.

close proximity to Sn, data shown in Table I. The respective lifetimes were calculated from those decays, using nonlinear least-squares impulse reconvolution analysis. We see both a reduced mean lifetime (τ_{mean} on 15 nm Sn=3.4 ns) and amplitude-weighted lifetime ($\langle\tau\rangle$ on 15 nm Sn=3.4 ns) for fluorophores near-to Sn as compared to the glass control sample (τ_{mean} on glass=3.9 ns and $\langle\tau\rangle$ on glass=4.1 ns). These findings of reduced fluorophore lifetimes are consistent with our previously reported findings for nanosecond decay time fluorophores sandwiched between silver nanostructures, similarly suggesting the radiating plasmon model[15,16] is a suitable description of the tin-fluorophore enhancement mechanism. In this description, the lifetime of the fluorophore-metal system is reduced due a faster and more efficient fluorophore-plasmon coupling and then coupled system, Table I (top, emission).

For tin-fluorophore combinations in this work, we suggest two complementary effects for the observed fluorescence enhancement: (i) surface plasmons can radiate coupled fluorescence efficiently, and (ii) an enhanced absorption or electric field facilitates enhanced emission. When a luminophore is placed near-to metal, there is often a very strong net absorption effect caused by the localized enhanced electromagnetic field of the incident excitation field. Since enhanced electromagnetic fields in proximity to metal nanoparticles are the basis for the increased system absorption in

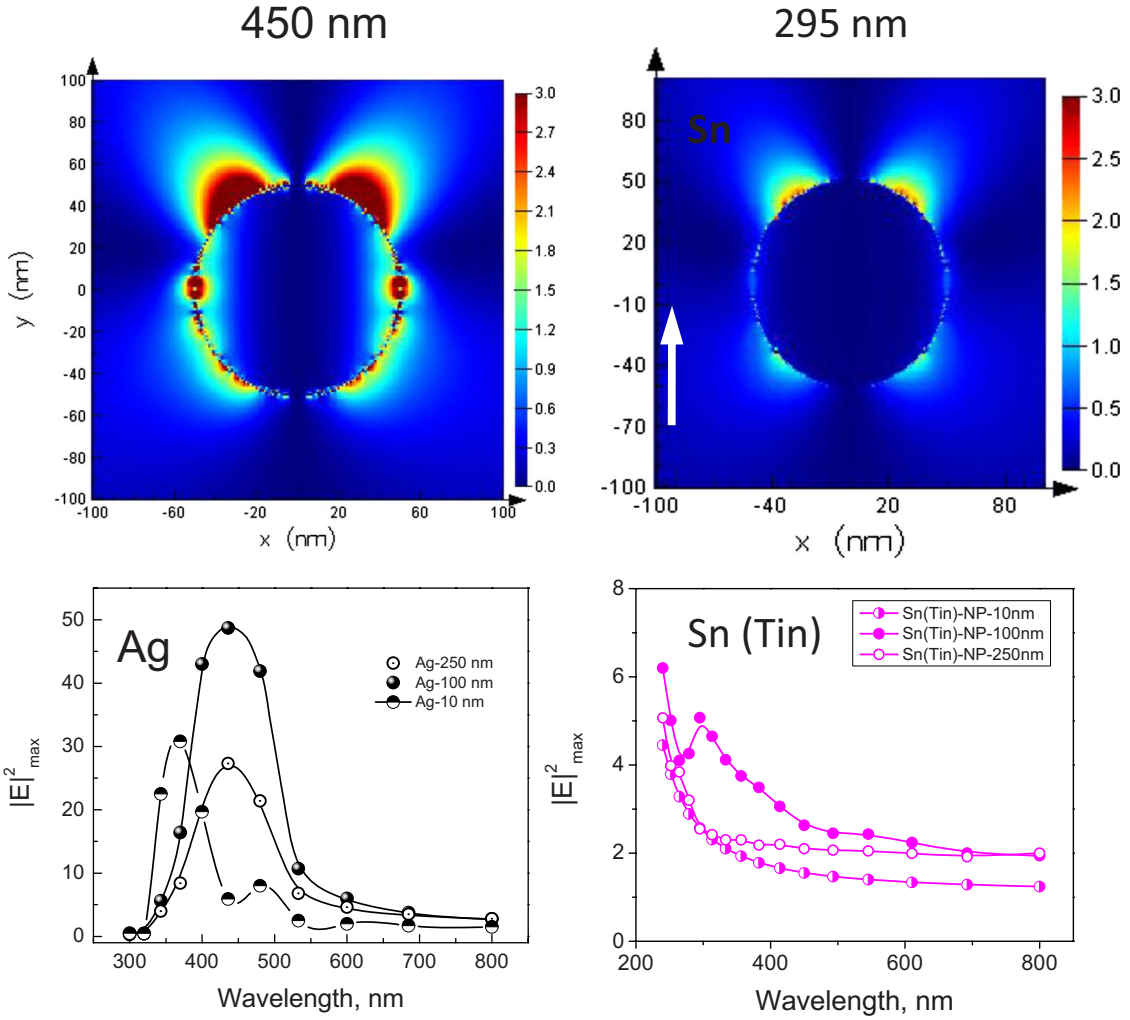

FIG. 5. (Color online) The dependence of electric field maximum intensity upon wavelength of the incident light (bottom). Calculations were undertaken using FDTD simulations for Ag and Sn nanoparticles of sizes, 10, 100, and 250 nm (diameter). (Top) image of a nearfield intensity distribution around 100 nm Sn nanoparticles taken at 295 nm (position of the local maximum) and for a 100 nm Ag particle taken at 450 nm. White arrow shows direction of the incident light injection. Finite difference time domain (FDTD).

MEF, we have additionally calculated the electric field distributions (using FDTD calculations) for tin nanostructures on a planar surface (Fig. 5). We are aware that the morphology of the actual particles is not exactly same, but we have chosen diameters of 10, 100, and 250 nm to simplify and indeed approximate the surfaces. FDTD calculations show that the maximum electric field intensity is predicted to occur in the UV range for tin. In contrast, for silver which is widely used in MEF,[15,17] the notable wavelengths/range occurs from 400 to 500 nm. From Fig. 5, we can also see that the magnitude of the electronic field in the same x and y planes is much more favorable in the blue/visible spectral regions. That said, the near-field enhancements observed around the tin nanoparticles, coupled with their low cost to deposit, makes the use of tin useful and attractive. It is also of interest to note the electric field versus wavelength profile for tin is more pronounced in the UV range, which may be important for the label-less intrinsic-fluorescence-based detection of proteins, work currently underway in our laboratory. To date, very few metals have been shown to be plasmon supporting materials in the UV, as reviewed in a recent paper in the context of surface plasmon coupled fluorescence spectroscopy,[18] hence tin nanoparticles may be an alternative to aluminum, which has been shown useful for MEF in the UV.

IV. CONCLUSIONS

In this letter, we report the first observation of MEF from tin substrates. When fluorophores are placed in close proximity to the tin substrates, MEF was observed. In addition, the decay times of fluorophores were also reduced near-to the tin substrates, suggesting both an enhanced electric field and a plasmon-coupling component is the mechanism for the observed fluorescence enhancement, similar to substrates made from silver, copper, and gold nanoparticles, reported by our laboratory in the past.

ACKNOWLEDGMENTS

The authors would like to thank the University of Maryland Biotechnology Institute and the Institute of Fluorescence for salary support.

[1]R. R. Alfano, G. C. Tang, A. Pradhan, W. Lam, D. S. J. Choy, and E. Opher, IEEE J. Quantum Electron. **23**, 1806 (1987).
[2]R. R. Chance, A. H. Miller, A. Prock, and R. Silbey, J. Chem. Phys. **63**, 1589 (1975).
[3]S. Choi, E. Y. Choi, D. J. Kim, J. H. Kim, T. S. Kim, and S. W. Oh, Clin. Chim. Acta **339**, 147 (2004).
[4]M. E. Cullum, L. A. Lininger, S. Z. Schade, S. E. Cope, J. C. Ragain, Jr., and L. G. Simonson, Mil. Med. **168**, 915 (2003).
[5]R. S. Davidson and M. M. Hilchenbach, Photochem. Photobiol. **52**, 431 (1990).
[6]C. D. Geddes and J. R. Lakowicz, J. Fluoresc. **12**, 121 (2002).
[7]K. Aslan, S. N. Malyn, and C. D. Geddes, Analyst (Cambridge, U.K.) **132**, 1112 (2007).
[8]K. Aslan, S. N. Malyn, and C. D. Geddes, J. Fluoresc. **17**, 7 (2006).
[9]Y. Zhang, K. Aslan, M. J. R. Previte, and C. D. Geddes, Appl. Phys. Lett. **90**, 173116 (2007).
[10]K. Aslan, M. J. R. Previte, Y. Zhang, and C. D. Geddes, J. Phys. Chem. C **112**, 18368 (2008).
[11]R. Pribik, K. Aslan, Y. Zhang, and C. D. Geddes, J. Phys. Chem. C **112**, 17969 (2008).
[12]Y. Zhang, A. Dragan, and C. D. Geddes, J. Phys. Chem. C **113**, 15811 (2009).
[13]Y. Zhang, A. Dragan, and C. D. Geddes, J. Phys. Chem. C **113**, 12095 (2009).
[14]K. Aslan, Y. X. Zhang, and C. D. Geddes, J. Appl. Phys. **103**, 084307 (2008).
[15]K. Aslan, Z. Leonenko, J. R. Lakowicz, and C. D. Geddes, J. Fluoresc. **15**, 643 (2005).
[16]J. R. Lakowicz, Anal. Biochem. **337**, 171 (2005).
[17]K. Aslan, J. R. Lakowicz, and C. D. Geddes, Anal. Bioanal. Chem. **382**, 926 (2005).
[18]K. Aslan and C. D. Geddes, Anal. Chem. **81**, 6913 (2009).